Received: 6 December 2017 | Revised: 18 May 2018 | Accepted: 24 May 2018

DOI: 10.1002/cmr.a.21438

SPECIAL ISSUE

WILEY

Compressed sensing: Reconstruction of non-uniformly sampled multidimensional NMR data

Mark Bostock | **Daniel Nietlispach**

Department of Biochemistry, University of Cambridge, Cambridge, UK

Correspondence
D. Nietlispach, Department of Biochemistry, University of Cambridge, Cambridge, UK.
Email: dn206@cam.ac.uk

Abstract

Nuclear magnetic resonance (NMR) spectroscopy is widely used across the physical, chemical, and biological sciences. A core component of NMR studies is multidimensional experiments, which enable correlation of properties from one or more NMR-active nuclei. In high-resolution biomolecular NMR, common nuclei are ^{1}H, ^{15}N, and ^{13}C, and triple resonance experiments using these three nuclei form the backbone of NMR structural studies. In other fields, a range of other nuclei may be used. Multidimensional NMR experiments provide unparalleled information content, but this comes at the price of long experiment times required to achieve the necessary resolution and sensitivity. Non-uniform sampling (NUS) techniques to reduce the required data sampling have existed for many decades. Recently, such techniques have received heightened interest due to the development of compressed sensing (CS) methods for reconstructing spectra from such NUS datasets. When applied jointly, these methods provide a powerful approach to dramatically improve the resolution of spectra per time unit and under suitable conditions can also lead to signal-to-noise ratio improvements. In this review, we explore the basis of NUS approaches, the fundamental features of NUS reconstruction using CS and applications based on CS approaches including the benefits of expanding the repertoire of biomolecular NMR experiments into higher dimensions. We discuss some of the recent algorithms and software packages and provide practical tips for recording and processing NUS data by CS.

KEYWORDS

compressed sensing, multidimensional nuclear magnetic resonance, non-uniform sampling, signal processing, sparse sampling

1 | INTRODUCTION

Nuclear magnetic resonance (NMR) spectroscopy is widely used as an atomic resolution structural technique across the physical, chemical, and biological sciences. Essential to the information content provided by NMR spectroscopy are multidimensional experiments, which correlate information from NMR-active nuclei allowing the identification of spin networks that are connected, for example, through bonds (*J*-coupling) or through space (NOE transfer).

All multidimensional experiments require an "indirect" evolution period where on successive repetitions of an experiment a delay time is increased by a certain, typically fixed increment, during which free precession of the spins is monitored. For each additional dimension, an extra indirect evolution period is required, and thus an *N*-dimensional NMR experiment will have $N-1$ independent incrementation (evolution) periods, typically known as the indirect dimensions. It is the requirement to sample the frequencies present in each of these "indirect dimensions" independently which

leads to the often lengthy experiment times required for multidimensional NMR. In biomolecular NMR, a typical 2D can be expected to take on the order of hours, 3Ds days and 4Ds weeks, a problem exacerbated by the shift to higher magnetic fields. The time-consuming requirement to sample the indirect dimensions independently therefore often results in experiments that have suboptimal resolution.

Consequently, for almost as long as multidimensional experiments have been employed, efforts to reduce the experiment times have been devised. The many approaches have focused on reducing the number of points recorded in each indirect dimension while acquiring the same, or higher resolution, and this is variously known as sparse sampling, non-uniform sampling (NUS) or undersampling of data. As discussed below, the Fourier transform (FT) can no longer be used to process undersampled data and subsequent efforts have focused on alternative approaches to reconstruct the frequency domain. Broadly speaking, these alternative reconstruction approaches fall into two categories; those which use non-uniform and nondeterministic sampling of the indirect dimensions, and those which have restrictions on the sampling pattern, that is, Nyquist sampling (eg, for linear prediction) or use a non-uniform deterministic sampling scheme, for example, coupled evolution for reduced dimensionality methods.[1] Methods which can use data with nondeterministic sampling are the most general and can typically reconstruct data from any of the categories.[2] The results of such alternative processing methods may either produce a full multidimensional spectrum, or alternatively the raw data may be analyzed to provide information on signal frequencies, for example, APSY,[3] GFT-NMR,[4] and PRODECOMP.[5]

Recently, compressed sensing (CS)-based reconstructions have joined the family of nondeterministic techniques which reconstruct a full frequency-domain spectrum. CS was developed in information theory,[6,7] although the underlying concepts have been known for many decades,[8] and has become popular in a wide range of fields including magnetic resonance imaging (MRI),[9,10] as well as diverse areas from astronomy and astrophysics,[11] to super-resolution microscopy[12] and computerized tomography,[13] as well as other spectroscopies, for example, optical spectroscopy.[14] The value of CS-based reconstructions for undersampled NMR data was demonstrated in 2011[15,16] and since then a range of applications, algorithms, and software packages has been developed for NMR spectroscopists.[17-26] In this article, we review FT sampling theory and explain the modifications used for NUS sampling. We highlight the challenges of reconstructing such NUS spectra, and explain the basic theory behind CS-based reconstruction approaches. We demonstrate the benefits of CS reconstructions of NUS data and review a number of commonly used CS algorithms, discuss suitable sampling strategies, and provide some practical tips for reconstructing data, as well as highlighting the various data processing packages available.

2 | FOURIER TRANSFORM AND NYQUIST THEORY

An NMR signal results from the precession of magnetization detected as an induced current oscillating at a given frequency, Ω, which can be represented as a complex exponential. The magnitude of this oscillating signal decays over time, due to relaxation phenomena and the characteristic lifetime of a spin is typically represented by its decay constant, R_2. For a complex multispin system, many signals of variable intensities and frequencies sum to give the overall appearance of the free induction decay (FID):

$$S(t) = \sum_{k=1}^{N} S_k \exp(-i\Omega_k t) \exp(-R_{2k} t) \tag{1}$$

where k represents each individual frequency component with amplitude S_k, oscillation frequency Ω_k, and decay rate R_{2k}.

The FID is a continuous function; however, NMR data acquisition detects a discrete signal, which is achieved by sampling the FID at regular intervals. The relationship between sampling rate and the frequency range that can be correctly represented is given by the Nyquist theorem which states that the maximum observable frequency is determined by the sampling rate, given by:

$$\mathrm{SW} = \frac{1}{\Delta t} \tag{2}$$

where Δt represents the time increment between sampled points, otherwise known as the dwell time. Signals with a frequency higher than the maximum observable frequency, $\pm$SW/2, will appear aliased at a lower frequency. This is illustrated in Figure 1 where it can clearly be seen that a sinusoid with a higher frequency (orange curve) than the maximum detectable frequency (based on the sampling rate, red squares) will be indistinguishable from a lower frequency signal, and will appear aliased in the spectrum. To correctly identify the higher frequency signal, the sampling rate must be increased (black crosses). Consequently, the Nyquist theorem determines the sampling rate required for NMR experiments.

In order to observe the contributing spectral frequencies, the FT is used to convert time-domain data (right-hand side (RHS) of equation 3) into the frequency domain (left-hand side (LHS) of equation 3). Hence the LHS is defined in terms of frequency, ω, and the RHS in terms of time, t. For a complex signal, the discrete FT is as follows:

$$S_k(\omega) = \sum_{n=0}^{N-1} S(n\Delta t) \exp(-2\pi i k n/N) \tag{3}$$

where Δt is the sampling interval, $S(n\Delta t)$ are complex numbers representing the time-domain signal at each time point,

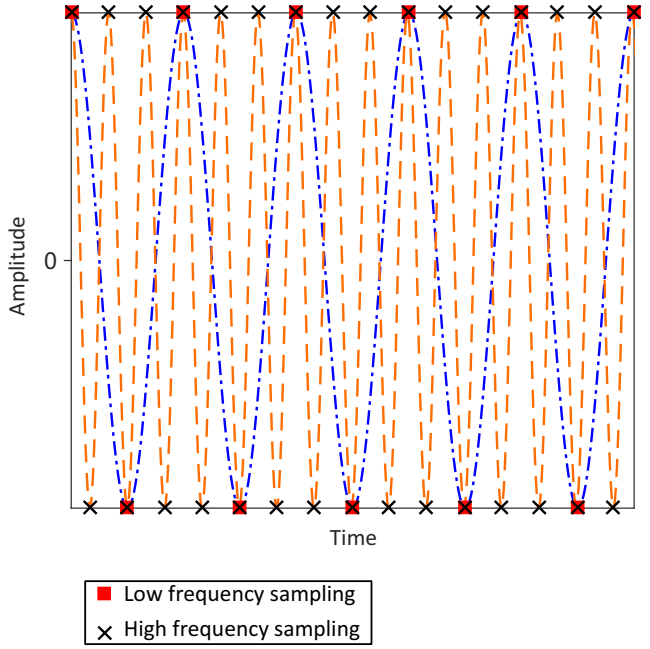

FIGURE 1 An illustration of the Nyquist theorem. A low frequency signal (blue) is defined by the sampling rate indicated by the red squares. However, a higher frequency signal (orange) cannot be defined by this sampling rate (red squares) and will be aliased to the frequency of the signal shown in blue. In order to correctly determine the frequency of the orange signal, sampling must be carried out at a higher rate, indicated by the black crosses

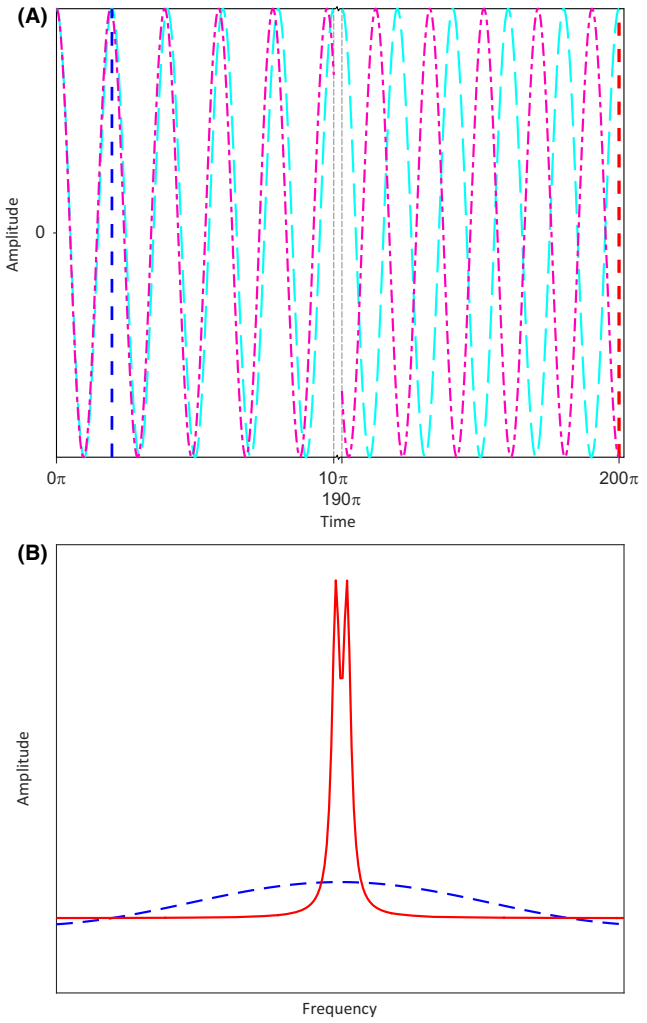

FIGURE 2 An illustration of resolution in NMR. In (A), the cyan and magenta signals can only be distinguished in the time domain as the acquisition time increases. This is illustrated for the frequency domain in (B) where the blue and red spectra use the data shown in (A) with t_{max} set at either the blue or red dotted lines respectively. When two curves are antiphase with respect to each other in the time domain, the two frequencies can be resolved

$S_k(\omega)$ is a series of complex numbers representing the frequency domain signal where $k \in [0, N-1]$, and Equation 3 is N-periodic in k. Thus, in addition to the requirement to sample at the Nyquist rate as discussed above, Equation 3 indicates that samples must be recorded uniformly, that is, for $N-1$ regularly spaced time intervals in order to preserve the orthogonality of the complex exponentials[27]:

$$\sum_{n=0}^{N-1} \exp(2\pi i(k-k')n/N) = 0,\ k \neq k' \tag{4}$$

Consequently, an NMR experiment requires a regularly spaced series of points to be acquired at the Nyquist sampling rates for each dimension, with all points sampled uniformly up to the maximum acquisition time. Ignoring the directly acquired dimension, for an N-dimensional experiment ($N-1$ indirect dimensions) with k_n points in the n^{th} indirect dimension, this amounts to acquisition of

$$2^{N-1} \times k_1 \times k_2 \times k_3 \times \ldots \times k_n \tag{5}$$

points in the indirect dimensions, or alternatively repetitions of the experiment. The factor of 2^{N-1} represents the requirement for frequency discrimination with a pure phase absorptive line shape, often implemented via quadrature detection, clearly demonstrating the rapid increase in sampling requirements with additional dimensions.

In addition to the requirements to sample regularly at the Nyquist rate, spectral resolution must also be considered. Spectral resolution is determined by the maximum acquisition time, which determines the ability to distinguish closely spaced peaks as shown in Figure 2. For a nondecaying signal, resolution can theoretically be increased indefinitely by sampling to longer acquisition times. However, due to the exponential decay term in Equation 1, in practice beyond a certain acquisition time, only noise will be detected. The natural linewidth of peaks, at half-maximal intensity, is given by:

$$L = \frac{R_2}{\pi} \tag{6}$$

Assuming the number of points (N) in the spectrum and time domain are the same (ie, assuming no zerofilling), the spectral resolution (Δf) is given by[28]:

$$\Delta f = L\left(\frac{\pi}{R_2}\right)\left(\frac{1}{N\Delta t}\right) = L\left(\frac{\pi R_2^{-1}}{t_{\max}}\right) \tag{7}$$

and $t_{\max}(= N\Delta t)$ is the maximum delay time in a given dimension. Equation 7 indicates that the optimum resolution is achieved when $t_{\max} \sim 3R_2^{-1}$ or $3T_2$; at this point, the resolution is determined by the natural linewidth, L. However, it has been shown that signal-to-noise (SNR) ratio only increases up to $t_{\max} \sim 1.26T_2$[28] and therefore collecting additional samples after this point to improve resolution will degrade the SNR. Consequently, using conventional, uniform sampling, maximum resolution cannot be achieved without substantially reducing SNR or conversely increasing the number of scans.

An additional consideration arises from the widespread introduction of high-field NMR spectrometers. For example, a typical $^{13}C\alpha$ dimension covering 20 ppm at

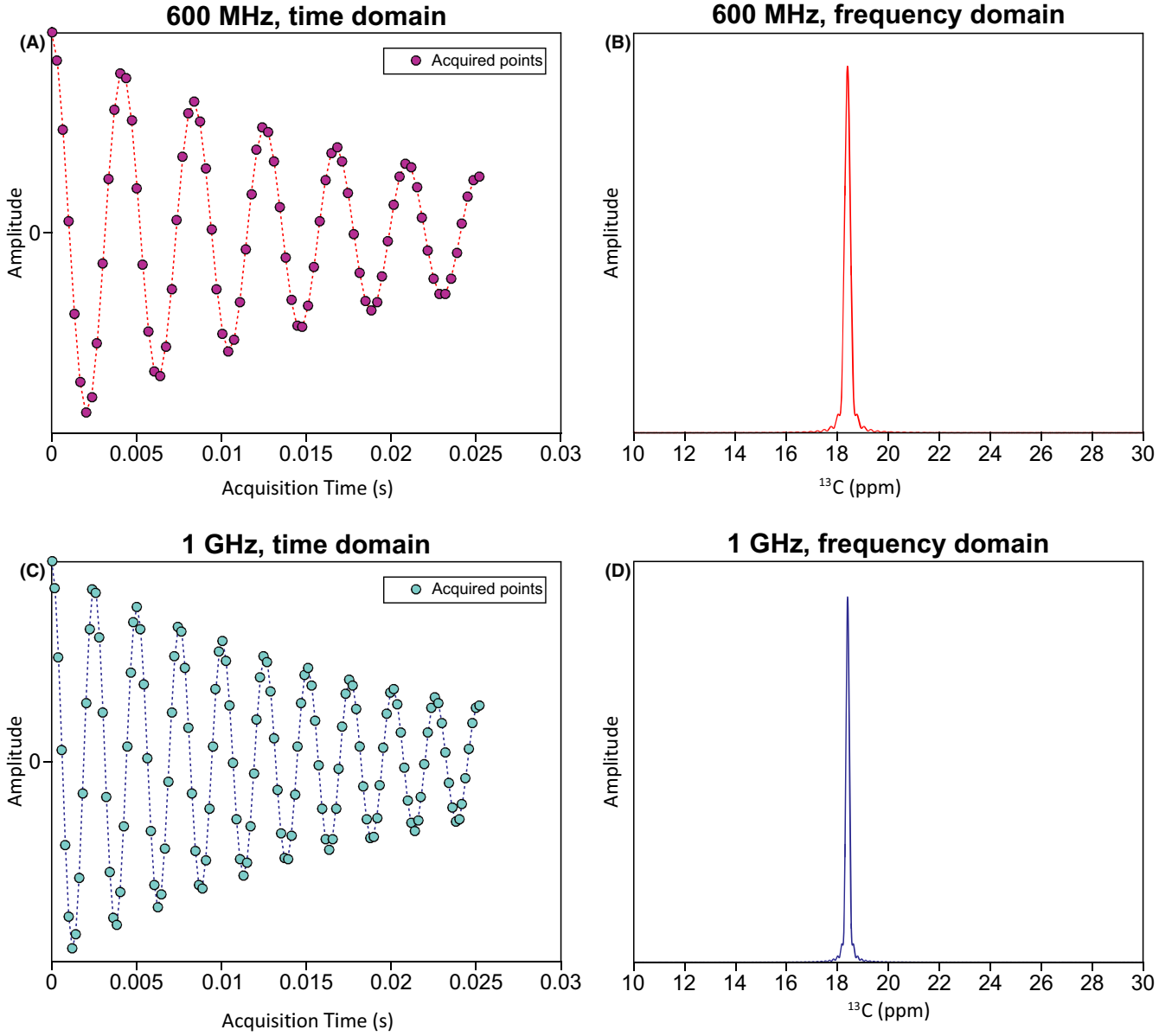

FIGURE 3 The effect of field strength on spectral sampling requirements. A ^{13}C signal is simulated, with a spectral width of 3000 Hz and $t_{\max}$ = 25.2 ms. Assuming uniform sampling, at 600 MHz this requires acquisition of 76 points i.e. Δt = 0.33 ms (A). This produces a spectrum with a frequency range of 20 ppm (B). To cover the same ppm range at 1 GHz requires a spectral width of 5000 Hz, corresponding to Δt = 0.2 ms, and thus 126 points to sample out to the same $t_{\max}$ (25.2 ms) (C). The signal in D, shows a narrower linewidth due to display on a ppm scale. The linewidth in Hz is unchanged.

600 MHz, corresponds to a frequency range of 3000 Hz requiring $\Delta t = 0.33$ ms. In the absence of any J_{CC} couplings and assuming sampling to $1.26T_2$, with R_2 ~50 Hz (T_2 = 20 ms), the dimension must be sampled out to t_{max} = 25.2 ms, that is, ~76 points. To acquire the same spectral width of 20 ppm at 1 GHz would require a frequency range of 5000 Hz and $\Delta t = 0.2$ ms. Assuming sampling to the same t_{max} (25.2 ms), ~126 points are required, a factor of 10/6 increase in sampling requirements (Figure 3). A similar effect will be observed for each indirect dimension, leading to an increase in the number of points by $(10/6)^{N-1}$ for an N-dimensional experiment in order to maintain the equivalent resolution at higher fields.

As a result of the challenges described above, the majority of high-dimensional experiments cannot be sampled appropriately to optimize both SNR and resolution.

3 | SAMPLING AND SENSITIVITY-LIMITED REGIMES

Two limiting regimes can be identified in NMR experiments, known as "sampling limited" and "sensitivity-limited" regimes.[29] In the former, the experiment time is determined by the need to sample out to high resolution in multiple indirect dimensions; SNR is assumed to be sufficient. In the sensitivity-limited regime, the limiting factor is the intrinsic sensitivity of the experiment or the sample concentration and so experiment time is typically spent acquiring sufficient scans to ensure appropriate SNR. The most likely scenario, however, is a compromise between these two regimes, with a trade-off occurring between experiment time, resolution, and SNR. For large proteins, this may result in poor quality spectra with significant overlap increasing the challenges for assignment and structural studies, and limiting the potential benefits of multidimensional experiments.

4 | NUS SAMPLING AND CONVOLUTION THEOREM

In order to circumvent the challenges discussed above, alternative approaches for sampling the indirect dimensions of multidimensional experiments were proposed in the early days of multidimensional NMR: Barna et al[30] suggested a randomized exponentially decaying sampling scheme concentrating most points at early evolution times where SNR is high, and sampling fewer points at long acquisition times to increase resolution. This approach has been developed by various authors but it was recently shown that randomization of the sampling schedule is essential for high-quality reconstructions,[2] while a modification of the exponential sampling approach which weights the gaps between acquired points according to a Poisson distribution has recently gained popularity.[31]

All such undersampling schedules allow a reduction in the total number of points required and hence experiment times, while potentially obtaining higher resolution. However, the FT can no longer be used to process data (Figure 4). This can be understood by considering the convolution theorem for FTs. In the following, t represents the time domain, ω the frequency domain, * indicates a convolution, and F is the Fourier transform:

$$F\{s(t) \cdot r(t)\} = S(\omega) * R(\omega) \tag{8}$$

In words, this indicates that the FT of the pointwise product of two time domain functions is the convolution of their FTs. We can consider an undersampled FID (with 0s replacing the missing data points) (Figure 4E) to be the product of a fully sampled FID (assuming N points regularly spaced according to the Nyquist theorem; Figure 4A) and a sampling schedule (Figure 4C) where 1s represent sampled points and 0s skipped points, and the number of sampled points, $M < N$. If we consider the equivalent frequency domain spectrum, using Equation 8, the FT of the undersampled FID (Figure 4F, red) is equivalent to the convolution of the FT of the fully sampled spectrum (Lorentzian lines; Figure 4B) with the point spread function (PSF, the FT of the sampling schedule; Figure 4D). The convolution is shown in blue in Figure 4F. The consequence, as indicated in Figure 4 is that every "real" peak in the undersampled spectrum introduces an artifact pattern resulting from the PSF. Clearly, as the number of "real" peaks increases, the artifact pattern becomes progressively more complicated. The aim of all nondeterministic reconstruction methods is to separate the "real" peaks from the PSF artifacts, which is often achieved by reducing the PSF artifact level. It should be noted that this can be further supported by choosing a sampling schedule that minimizes the intensity of artifacts in the PSF as this will also lead to a reduced artifact level in the final reconstruction.

5 | NUS RECONSTRUCTION METHODS

Since the earliest application of NUS approaches, a wide range of reconstruction methods has been proposed to overcome the limitation of the FT. The simplest approach, as described above, is to replace the "skipped" data points with 0s and then use the discrete FT. This is an example of a non-uniform discrete Fourier transform (nuDFT) and is equivalent to minimizing the ℓ_2-norm (Equation 9) for the spectrum (Parseval's theorem).[20]

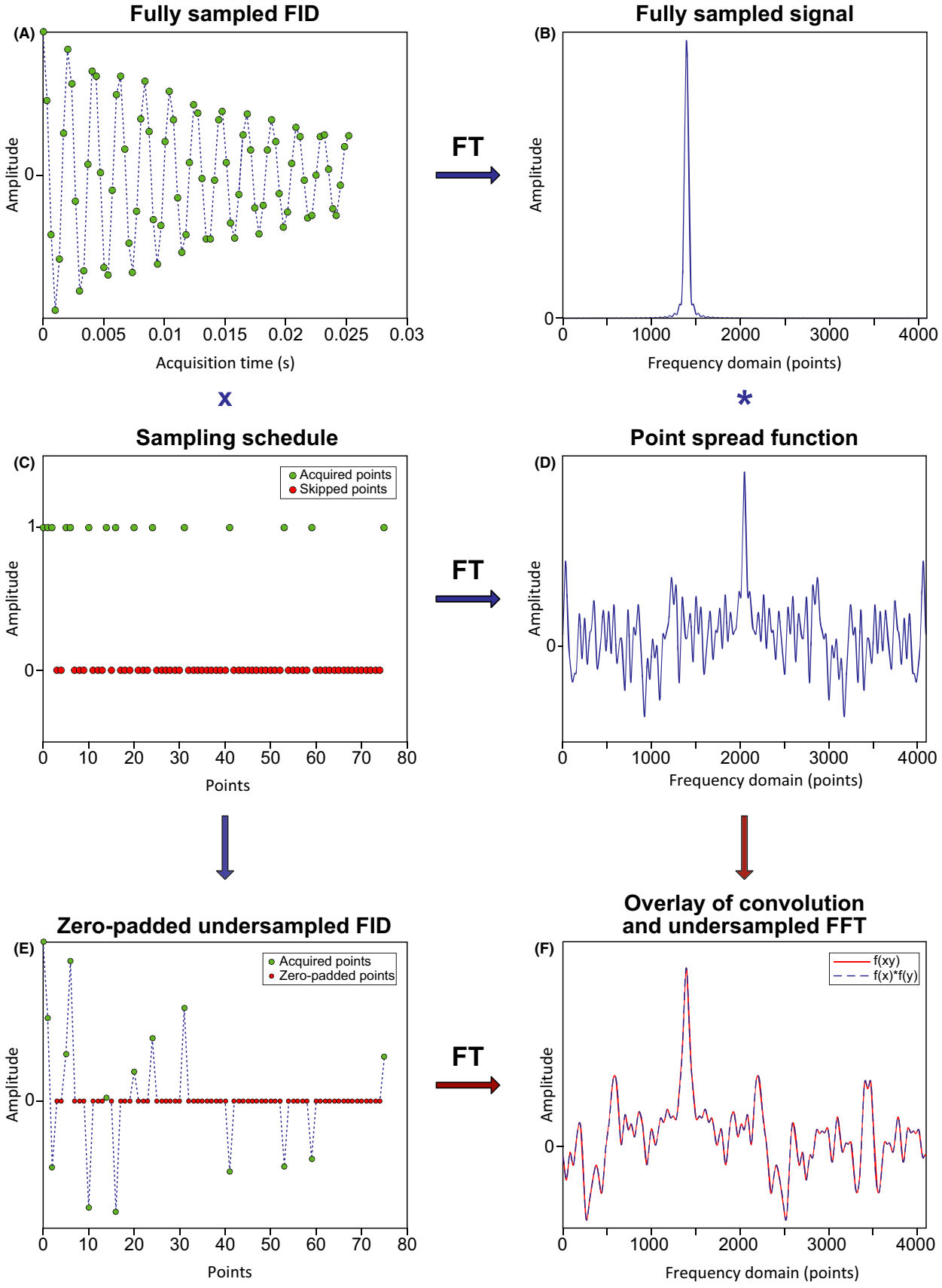
Fully sampled FID
(A)
Amplitude
0
0 0.005 0.01 0.015 0.02 0.025 0.03
Acquisition time (s)
FT
Fully sampled signal
(B)
Amplitude
0
0 1000 2000 3000 4000
Frequency domain (points)
x
*
Sampling schedule
(C)
Acquired points
Skipped points
1
Amplitude
0
0 10 20 30 40 50 60 70 80
Points
FT
Point spread function
(D)
Amplitude
0
0 1000 2000 3000 4000
Frequency domain (points)
Zero-padded undersampled FID
(E)
Acquired points
Zero-padded points
Amplitude
0
0 10 20 30 40 50 60 70 80
Points
FT
Overlay of convolution and undersampled FFT
(F)
f(xy)
f(x)*f(y)
Amplitude
0
0 1000 2000 3000 4000
Frequency domain (points)

FIGURE 4 An illustration of the Fourier transform convolution theorem in NMR spectroscopy. A fully sampled free-induction decay (FID, time domain) (A), is processed using the Fourier transform (FT) to produce a Lorentzian line shape (B), in the frequency domain. Undersampled data is recorded according to a sampling schedule (C), where 1s represent acquired points and 0s skipped points. Applying the FT to the sampling schedule (vector of 1 and 0 second) produces the point spread function (PSF) (D), which has an intense peak at the centre of the spectrum as well as artifacts from the undersampling pattern. An undersampled dataset which has been zero-padded by replacing the missing time points with zeros (E), is equivalent to the product of the fully-sampled FID and the undersampling pattern i.e. (A) × (C) = (E). The spectrum resulting from the FT of the undersampled data (E) is shown in F in red, i.e. $F\{(A) \times (C)\}$. This is equivalent to the convolution of the point spread function and the fully sampled frequency domain spectrum, i.e. (B)*(D) = (F) (blue curve).

$$||\mathbf{x}||_2 = \left(\sum_i |x_i|^2\right)^{\frac{1}{2}} \tag{9}$$

A range of subsequent nuDFT algorithms uses the predictability of the artifact pattern to remove artifacts from the most intense peaks and to reveal weaker peaks. Repeated iteratively, this can effectively clean up an undersampled spectrum. Examples of this approach include the MFT method,[32] FFT-CLEAN, based on earlier work in radio-astronomy,[33,34] SCRUB,[35] and the signal separation algorithm (SSA).[36]

Reconstruction using maximum entropy (MaxEnt) was introduced into NMR in the 1980s[37] with early application to undersampled data,[30,38] and more recently, the value of MaxEnt for 3D data was demonstrated.[39] Maximum entropy reconstruction has been reviewed in detail previously[40] and also in this journal.[41]

Another popular approach is multidimensional decomposition (MDD), which is based on fitting 1D vectors to experimental data,[42-44] with later developments including recursive MDD (rMDD)[45] and coupled MDD (Co-MDD).[46]

Another class of methods involves taking projections through a multidimensional dataset via coupled evolution of the indirect dimensions (radial sampling) and reconstructing either a full spectrum or peak lists based on this information. These methods include reduced dimensionality,[47] projection reconstruction,[48] GFT-NMR,[4,49] and APSY[3] among others. Recently, it was shown that reconstructing full spectra from radial samples introduces artifacts specific to the projection sampling, which can be reduced by further randomization of the sampling schedule.[2] Analysis of such projections is particularly useful for high dimensionalities. Many other methods have been introduced over the years which are discussed in other reviews.[1,50]

In recent years, an approach to full-spectrum reconstruction from undersampled data, developed in information theory, has been proposed based on CS theory.[6-8] CS has become popular in a number of fields, notably in MRI.[9] CS reconstructions have similarities to approaches such as CLEAN[34] but are based on a rigorous mathematical theory and consist of a family of algorithms with varying properties. In what follows, we discuss basic CS theory, give examples of some of the most promising algorithms available and discuss practical approaches for successful CS reconstructions of undersampled NMR data.

6 | CS THEORY

In this section, we provide a brief introduction to the theory underpinning CS reconstructions. Using matrix notation, NMR data can be represented as a system of linear equations:

$$\mathbf{Ax} = \mathbf{b} \tag{10}$$

where $\mathbf{x}$ represents the frequency domain, $\mathbf{b}$ the time domain, and $\mathbf{A}$ is the inverse FT. For fully sampled data, $\mathbf{A}$ is an $M \times N$ matrix, and $\mathbf{x}$ and $\mathbf{b}$ are vectors of length N and M, respectively, where $M = N$. Consequently, Equation 10 has a unique solution. However, for undersampled data, $M < N$ and thus Equation 10 is incompletely determined and has no unique solution. The challenge for all reconstruction techniques handling undersampled data is to find the "right" solution when Equation 10 is underdetermined. This is typically achieved by introducing additional assumptions, for example, maximizing the entropy, knowledge about regions with/without peaks etc.

Compressed sensing theory assumes that $\mathbf{x}$ can be reconstructed exactly by minimizing the ℓ_0-"norm" for $\mathbf{x}$, equivalent to choosing the sparsest solution:

$$\min_{\mathbf{x}} ||\mathbf{x}||_0 \text{ subject to } \mathbf{Ax} = \mathbf{b} \tag{11}$$

where the ℓ_0-"norm" is:

$$||\mathbf{x}||_0 = \sum_i |x_i|^0 \tag{12}$$

It can be clearly seen that this is equivalent to counting the number of non-zero elements, assuming that we define $0^0 = 0$,[7] and thus by minimizing this function, we will minimize artifacts generated by convolution with the PSF. Assuming $\mathbf{x}$ is k-sparse, we can reconstruct this from $\mathcal{O}(k)$ random points, where k-sparse is defined as having no more than k non-zero components. However, the solution to Equation 11 is typically not computationally tractable[51] and so is not a practical

solution. Nevertheless, CS theory states that by taking slightly more samples, minimizing the ℓ_1-norm, which is solvable using readily available algorithms, gives the same solution:

$$\min_{\mathbf{x}} ||\mathbf{x}||_1 \text{ subject to } \mathbf{Ax} = \mathbf{b} \tag{13}$$

where the ℓ_1-norm is given by:

$$||\mathbf{x}||_1 = \sum_i |x_i|^1 \tag{14}$$

which is equivalent to the sum of all the points in $\mathbf{x}$. (More information about norms is found in Box 1.) In this case, the sampling requirement has the following relationship[6]:

$$M \geq Ck \log N \tag{15}$$

Box 1

Norms

A norm uses a certain criterion to assign a positive length to a vector (aside from the 0 vector). Different norms use different criteria to define the lengths of vectors. The ℓ_2-norm (sometimes known as the Euclidian norm) is the "ordinary distance" from the origin to a point and is given by a generalization of Pythagoras' theorem. For complex numbers, the complex modulus is used, $|x_k| = \sqrt{x_k^* x_k}$. The ℓ_2-norm is defined as:

$$|\mathbf{x}| = \sqrt{\sum_{k=1}^{n} |x_k|^2} \tag{17}$$

The vectors satisfying a given value of the ℓ_2-norm in 2D map out a circle of radius $|\mathbf{x}|$ and by extension an n-sphere for an n-dimensional vector.

The ℓ_1-norm is sometimes known as the Taxicab or Manhattan norm and in 2D reflects the distance from an origin to a point using a rectangular grid. The ℓ_1-norm is defined as:

$$||\mathbf{x}||_1 = \sum_{i=1}^{n} |x_i| \tag{18}$$

The set of vectors satisfying a given constant for the ℓ_1-norm map out a square with vertices lying on the coordinate axes. For a radius of 1, this is defined by $|x| + |y| = 1$.

The ℓ_0-"norm"[7] is not a true norm and requires the definition $0^0 = 0$. Hence, this represents the number of non-zero entries in a vector.

Finally, the ℓ_p-norm is given by:

$$||\mathbf{x}||_p = \left(\sum_{i=1}^{n} |x_i|^p \right)^{\frac{1}{p}} \tag{19}$$

For $0 < p < 1$, the p-norm is not a true norm since it no longer satisfies the triangle equality that the length of the sum of two vectors is less than or equal to the sum of the lengths of the two vectors: $p(\mathbf{x} + \mathbf{y}) \leq p(\mathbf{u}) + p(\mathbf{v})$. However, we will find this is useful as an approximation to the ℓ_0-"norm".

In Equation 15, C is a universal constant, which depends mostly on the reconstruction algorithm. In general, C is difficult to calculate and this is rarely done. Theoretically k-sparsity assumes recovery of k non-zero elements. In reality most situations are not truly sparse, but instead are compressible, that is, k significant coefficients which should be recovered. k thus represents points rather than peaks. While it is not possible to use Equation 15 to predict the exact number of samples required for a given spectrum, and it should also be noted that Equation 15 represents a lower bound, it can be used to understand the general sampling requirements. Since Equation 15 has a log dependence on the size of the spectrum ($\mathbf{x}$), this indicates that the primary determinant of the required number of samples, M, is the sparsity of the spectrum, k, not its final size. We will see the great benefit of this later.

NMR spectra cannot be solved exactly using Equation 13. Instead, this is typically modified to take account of noise in the spectrum by relaxing the constraint giving:

$$\min_{\mathbf{x}} ||\mathbf{x}||_1 \text{ subject to } \mathbf{Ax} - \mathbf{b} \leq \delta \tag{16}$$

where δ is an estimate of the noise in the data.

Thus, in order to consider CS reconstruction of an undersampled spectrum, the spectrum must be sparse and sampled with an incoherent sampling scheme, that is a randomized schedule to minimize aliasing artifacts. It is important to keep these two factors in mind when considering M, the appropriate sampling fraction to record.

7 | CS ALGORITHMS

A variety of algorithms is available for CS processing of NMR spectra. Broadly speaking, these can be divided into two groups: those which minimize the ℓ_1-norm, similar to Equation 13, and those which minimize a reweighted p-norm where $p \leq 1$, potentially allowing an approximation to the ℓ_0-"norm". In the former category are algorithms such as iterative soft thresholding (IST) and iterative hard thresholding (IHT), while the latter category includes the iteratively reweighted L1 (IRL1) and least squares (IRLS) implementations. Other target minimization functions have also been suggested, for example, Gaussian-smoothened ℓ_0-"norm"[52] but these have not gained widespread use. IST exists in two main flavors in the NMR literature[23,52] either providing strict accordance with the measured data at each iteration (IST-S),[16,52,53] or keeping a balance between sparsity and measured data (IST-D).[19,54] The IST algorithm used by the authors in[18] is similar to the IST-S algorithm, while the IHT algorithm is similar to the IST-D approach, but with a hard threshold. Subsequent modifications in the Cambridge CS software (see Data processing section) are a combination of the IST-S and IST-D approaches. Along with IHT, these algorithms all use a thresholding approach to extract "true" signals and then an inverse FT step (IFT) to remove the contribution from these components, and the contributing noise due to the convolution of these signals with the PSF. Repeated iteration leads to a spectrum with considerably reduced artifacts. Thus, these methods give comparable results. Clearly a key consideration for such iterative algorithms is convergence.[53] Various stopping criteria have been suggested ranging from very simple approaches, for example, a maximum number of iterations, through to more sophisticated approaches which may aim to detect when the residual contains only noise or when no new signals are being added to the spectrum. Many of the available software packages contain automated stopping criteria which typically perform well, however, reconstruction quality may be improved in some cases by altering these criteria.

The reweighted approaches reformulate the ℓ_1 minimization into a weighted minimization,[52,55] for example, for IRL1:

$$||\mathbf{x}||_1 = \sum w_i x_i \tag{20}$$

where:

$$w_i^{n+1} = \frac{1}{|x_i|^n + \varepsilon} \tag{21}$$

n represents the iteration number and ε is used to avoid dividing by 0. In the IRLS approach[16,23,56] weights are set to:

$$w_i = |x_i|^{p-2} \tag{22}$$

Thus, in IRLS, the weighted norm allows the p-norm to be expressed as an ℓ_2-norm which can then be solved as a least squares problem:

$$||\mathbf{x}||_p^p = \sum_i |x_i|^p \tag{23}$$

$$||\mathbf{x}||_p^p = \sum_i w_i |x_i|^2 \tag{24}$$

An additional modification[57] allows the p-value to be reduced on successive iterations enabling an approximation to the ℓ_0-"norm". Although IRLS is more computationally demanding, and thus typically slower than IST, it has been suggested that it provides better reconstructions at lower sampling levels.[20,58,59] Applications using these two main groups of algorithms will be discussed further below.

More recently, low-rank reconstruction has been proposed as a high-fidelity algorithm suitable for reconstructing NMR spectra, in particular for low

intensity, broad peaks.[60,61] The low-rank approach attempts to reconstruct a spectrum with the fewest peaks, compared to CS which minimizes the number of non-zero values, and is independent of the line widths of the peaks. Low-rank reconstruction solves the following equation:

$$\min_{\mathbf{x}} ||\mathbf{Rx}||_* + \frac{\lambda}{2}||\mathbf{y} - \mathbf{Ux}||_2^2 \quad (25)$$

where $\mathbf{y}$ is the undersampled time-domain data, $\mathbf{x}$ is the fully sampled time-domain signal, and $\mathbf{U}$ is the undersampling operator, converting a fully sampled FID to an undersampled FID. $\mathbf{R}$ converts $\mathbf{x}$ to a Hankel matrix, $\mathbf{X} = \mathbf{Rx}$, where $\mathbf{X}$ is low-rank. The nuclear norm, $||\mathbf{Rx}||_*$, or sum of the matrix's singular values,[62] represents the number of frequency oscillations in the FID and thus quantifies the number of peaks in the spectrum. λ balances the data consistency term with the low rank term. Results suggest that low rank reconstruction provides greater fidelity for broad, low intensity peaks than CS reconstruction. By assuming sparsity in terms of peaks rather than values, low-rank reconstruction is very well adapted to NMR spectra, which become strictly sparse under this assumption.[23] However, to date, available implementations of the low rank method are slower than other CS algorithms and limited to 2D data, although more recent algorithms have demonstrated extension of this approach to higher dimensional spectra $\geq$ 3D.[61]

8 | COMPRESSED SENSING: EXAMPLES AND ITS BENEFITS

Early work with applications to a range of 2D and 3D experiments demonstrated the fidelity of the reconstruction method in terms of peak positions and peak intensity.[15,16] In the context of triple resonance experiments, CS was shown to provide improved reconstruction of weaker peaks, compared to an existing MaxEnt implementation.[15] Subsequently, application to 3D ^{15}N NOESY experiments was demonstrated, which present a particular challenge due to the high dynamic range and substantial overlap of signals and the requirement to accurately reconstruct the intensities of the information-rich weaker cross-peaks.[18,19] A variety of ℓ_1-norm minimization algorithms were shown to provide fast and accurate reconstructions of NOESY data across a range of peak intensities, with the required sampling fraction dependent on the complexity of the spectrum as expected from Equation 15. An example reconstruction of a 3D ^{1}H,^{15}N NOESY-HSQC for the membrane protein sensory rhodopsin II (pSRII) is shown in Figure 5 using the IHT algorithm, demonstrating the fidelity of intensity and peak reconstruction.

A long-standing benefit of NUS techniques is to enable improved resolution by allowing sampling to considerably higher $t_{1\max}$ values than would otherwise be accessible using an equivalent uniformly sampled FT-processed version. This was proposed as a key benefit of NUS approaches in the early days of NUS methods[38] and has been previously demonstrated in the context of MaxEnt reconstructions of 3D-NUS triple resonance spectra.[39] Nevertheless even using NUS approaches, triple resonance 3D backbone experiments are still typically recorded with modest spectral resolution due to time constraints. Recently a detailed comparison[63] was made to investigate different approaches for extending resolution in multidimensional experiments focussing on linear prediction or IST-based[53] extrapolation of uniformly sampled data vs IST reconstruction of NUS data sampling out to high resolution, combined with further IST based extrapolation (up to maximum $4*T_2$), demonstrating the benefits of combined CS-based interpolation and extrapolation. The authors suggest that optimum sensitivity, resolution, and frequency reconstruction are achieved by acquiring data to $0.5*T_2$ with further improvements to linewidth by extrapolating to $2*T_2$. Although this study focussed on the hmsIST processing method it is likely that the recommendations are more general, and are indicative of resolution improvements that can be accessed with CS-NUS reconstructions. Figure 6 shows a comparison of two time-equivalent 3D NUS-HNCA semi-constant time experiments[64] recorded on a 0.5 mmol/L sample of OppA (^{2}H,^{13}C,^{15}N), a 60 kDa

FIGURE 5 Comparison of CS and FT reconstructions of a 3D [^{1}H,^{15}N] NOESY experiment for a 1 mM U-[^{1}H,^{15}N]-labelled sample of the D75Q mutant of sensory rhodopsin II (pSRII-D75Q), recorded with a $t_{1,\max}$ of 13.1 ms (^{1}H) and 13.4 ms (^{15}N) (spectral widths of 8403 Hz and 2530 Hz in the ^{1}H and ^{15}N dimensions respectively). Two strips are shown illustrating the quality of reconstruction in both more (65Glu) and less (64Ala) crowded regions of the spectrum. Side-chain and amide regions are displayed. The fully-sampled (110* × 34*) FT-processed spectrum is shown in C, (blue) with ns = 40 (experiment time ~9 days). CS processing using the IHT algorithm with a 40% sinusoidal poisson schedule is shown in B, (red) (ns = 40, experiment time ~3.5 days). A time-equivalent fully-sampled FT-processed spectrum (ns = 16) is shown in A, (magenta). 1D slices taken along the dotted lines in A–C are shown in D. The quality of the CS-reconstruction compared to the FT spectra is clear, indicating that the time-saving could be used for example to enhance spectral resolution by sampling out to longer $t_{1,\max}$. Spectra were recorded at 308 K on a Bruker AV800 spectrometer equipped with a 5 mm TXI HCN/z cryoprobe.

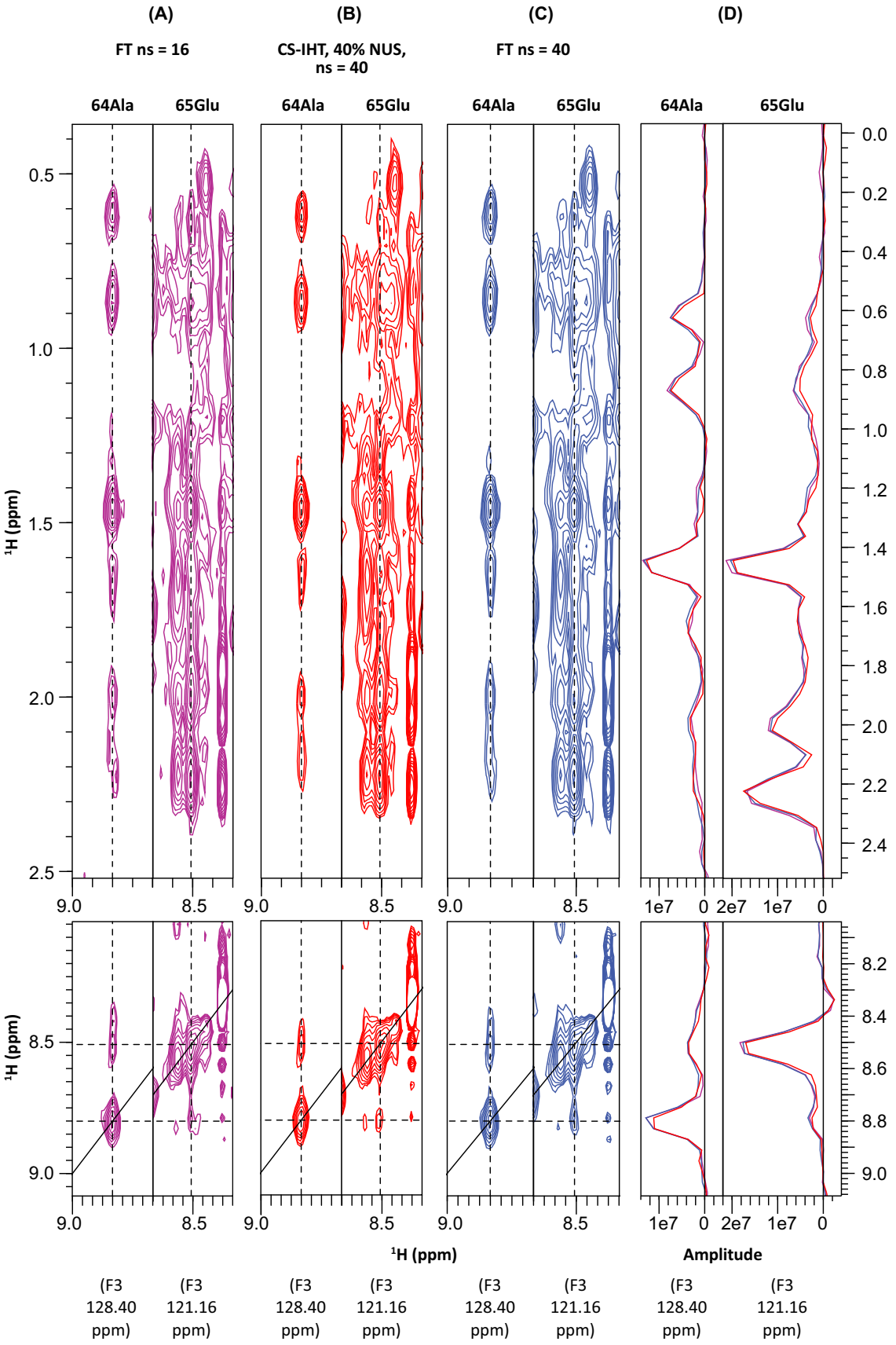

protein with a correlation time of 29 ns at 298 K. Each experiment was recorded for 7 hours using NUS to acquire a combined total of 350* complex points in the ^{15}N and ^{13}C indirect dimensions. Three reconstructions are shown in Figure 6. A low-resolution NUS CS-reconstructed experiment (^{15}N t_{1max} of 12.2 ms equivalent

FIGURE 6 Comparison of two time-equivalent 3D NUS TROSY-HNCA semi-constant time experiments recorded on a 0.5 mM sample of OppA (^{2}H, ^{13}C, ^{15}N). The correlation time of OppA at 298 K is 29 ns resulting in an average T_2 relaxation time for the TROSY line of ~48 ms. Each experiment took 7 hours to record with 350* combined ^{15}N,^{13}C complex points in the indirect dimensions. The spectra were reconstructed using the CS-IHT algorithm in the Cambridge CS software. [^{1}H, ^{15}N] (A) and [^{1}H, ^{13}C] (B) strip plots are shown for residues 106Ala and 213Asn, which are partially overlapped in the ^{1}H and ^{15}N dimensions. Three CS-reconstructed spectra are shown: (Magenta) A low resolution spectrum using a 22% Poisson gap sampling schedule, resulting in a ^{13}C $t_{2\max}$ of 8 ms (50* complex points) and a ^{15}N $t_{1\max}$ of 12.2 ms (32* complex points, equivalent to 0.25*T_2). (Green) The data for the spectrum shown in red is extended in the ^{15}N dimension to 24.4 ms (64* complex, 0.5*T_2) and reconstructed using CS-IHT. This results in a spectrum of moderately improved resolution. Further improvements could be gained by extrapolating the ^{15}N dimension to longer $t_{1\max}$ using the same approach. (Cyan) Instead, in this example, a second higher resolution spectrum was recorded with a $t_{1\max}$ of 60 ms (158* complex points, 1.25*T_2) and the resolution in the ^{13}C dimension unchanged. 350* complex points (Poisson gap sampling) were obtained as before, equivalent to 4.4% sampling. A, The dramatically increased resolution resulting from the extended ^{15}N time dimension is shown (cyan). B, The increased resolution in the ^{15}N dimension (cyan) enables the separation of the cross peaks of residues 106Ala from those of 213Asn as shown in the [^{1}H,^{13}C] strip plots. Break-through contributions from the neighbouring planes that make the assignment process ambiguous at lower resolution (magenta, green) are marked with (*). C, The increase in resolution, even to 1.25*T_2 does not significantly deteriorate the signal-to-noise ratio. Experiments were recorded at 298 K on a Bruker AV800 spectrometer equipped with a 5 mm TXI HCN/z cryoprobe.

to 0.25*T_2) (magenta) is further extrapolated to ^{15}N $t_{1\max}$ = 24.4 ms (0.5*T_2) (green) using CS-IHT reconstruction leading to a moderate resolution improvement that partly results from the shift of the apodization function toward the later time points. Further reductions in linewidth could be achieved by extrapolation to even longer $t_{1\max}$ values. In this case, however, higher resolution was obtained in a second experiment by altering the sampling schedule to acquire up to $t_{1\max}$ = 60 ms (1.25*T_2) in ^{15}N. The improvement in linewidth in Figure 6A is considerable (cyan) and the benefit is demonstrated in Figure 6B where peak contributions from different residues are now clearly separated due to the higher ^{15}N resolution, removing the ambiguity in assigning the two residues shown. While the increase in resolution reduces ambiguities in spectral assignment, sampling to this longer $t_{1\max}$ does not substantially alter the SNR (Figure 6C), measured as a signal-to-threshold ratio relative to the contour level at which peaks can be recognized with sufficient confidence.[15]

As discussed above, the available CS algorithms can be divided into convex and nonconvex minimizations. IRLS has proved particularly popular from the nonconvex minimization class with applications including measurement of scalar and residual dipolar couplings[24] as well as in more traditional undersampled spectra.[16,65] It is suggested that use of IRLS may allow the optimal solution to be found with fewer measurements than for the ℓ_1-norm[58] and in some cases may outperform IST, although IST has lower computational requirements, which may be an important consideration for large datasets.[20] Further improvements in reconstruction quality may be obtained with the addition of virtual echo reconstruction.[22]

More recently, a number of authors have suggested reducing the number of quadrature components acquired per time coordinate by random acquisition of quadrature components. This is variously known as random phase detection (RPD), random quadrature detection (RQD), and partial component sampling[66,67] and has also been implemented in the context of CS reconstructions with extension to gradient-selected experiments.[17] This gives further flexibility in the design of sampling schedules, allowing bias of the sampled points toward time, rather than quadrature components.

9 | HIGHER DIMENSIONS

Typical uses of CS reconstructions allow improved resolution and SNR and/or time savings for existing NMR experiments. Consequently, CS, along with other NUS-based reconstruction methods facilitates the use of higher dimensional experiments. A range of higher dimensional experiments (> 4D) has been proposed, including some with dedicated processing methods.[34,35,43,46,68-72] Here, we focus on the advantages of 4D experiments over existing 3D experiments. Although 4D experiments existed before the widespread use of NUS, undersampling techniques allow their full potential to be achieved by extending $t_{1\max}$, while still acquiring the experiment in a reasonable amount of time. As shown in Equation 15, sampling requirements scale approximately as $k\log(N)$. As described in the section "CS theory", k-signals refers to k significant components in the reconstruction domain and thus a single peak will be described by a number of signals. Since in typical NMR situations, the direct dimension is fully sampled and processed with the FT, and CS reconstructions are usually carried out as separate reconstructions of the $n-1$ indirect dimensions for each point in the direct dimension, N is therefore the number of points in the indirect dimensions of the reconstruction (frequency) domain. In addition, this means that the sparsity will be affected by the distribution

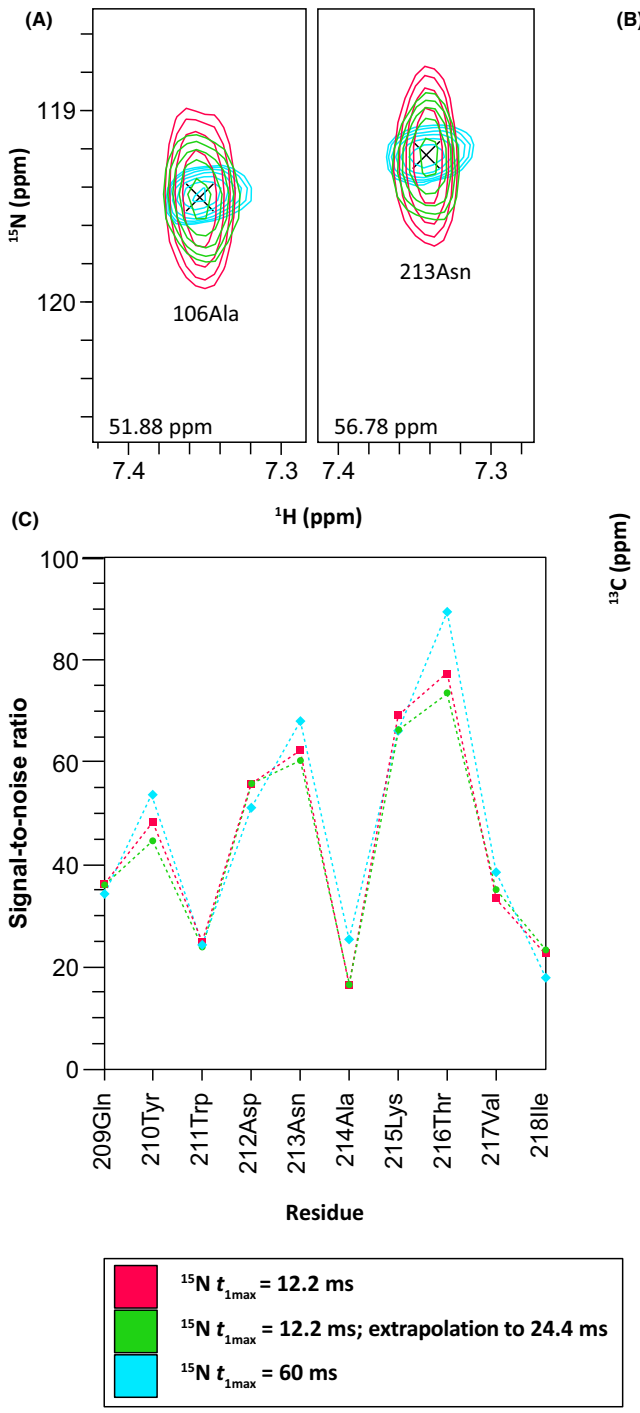

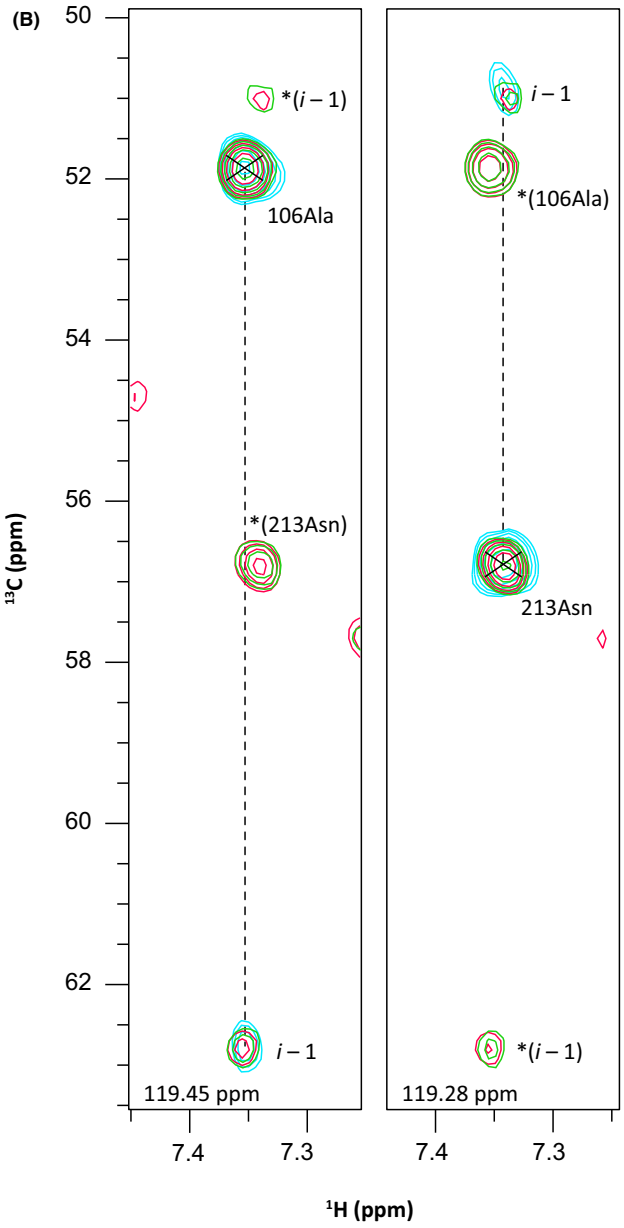

of signals across the direct dimension. Although k is difficult to predict in practical situations and C in Equation 15 is not usually known, we nevertheless use the form $k\log(N)$ with hypothetical values for illustrative purposes. Taking the example of a 3D experiment with $k = 1000$ and $N = 128 \times 128 = 16384$ points, approximately 4200 measurements need to be made across the indirect dimensions, that is, 25%. Based on practical experience, we and others observe substantially lower sampling requirements for 4D spectra.[19] This can be explained using Equation 15 assuming that on separating the data into a fourth dimension there is no substantial change in k. This assumption is reasonable as each peak observed in the 3D experiment will only occupy a small fraction of the additional planes in the fourth dimension. Therefore, taking $k = 1000$ again and $N = 128 \times 128 \times 128$, 2097152 points would be required for an FT experiment, but only 6300 measurements required for an NUS experiment with CS reconstruction, that is, 0.3% sampling. Even accounting for a small increase in k, this still brings recording times for 4D

experiments into the region of a 3D, while allowing substantially longer t_{1max} values for the indirect dimensions compared to time-equivalent fully sampled experiments. Importantly, through NUS, 4D experiments can be recorded with good resolution in a realistic time frame while the fully sampled versions necessitate a substantial reduction in resolution that limits their usefulness.

The addition of a fourth dimension can provide many opportunities, for example, by reducing ambiguity in assignments due to the addition of an extra frequency axis and reducing strong overlap, for example, for large proteins. An example of an NUS 4D HCCH NOESY experiment, recorded on a highly deuterated selectively ^{13}C ILVA-labeled methyl-protonated sample is shown in Figure 7, using 1000 points from 12480 complex points and 40 scans, equivalent to 8% sampling, with an experiment time of ~4.5 days. This example emphasizes that a high-quality 4D NOESY can be recorded in under 5 days. Although a relatively moderate resolution was chosen in this example, the resolution could be improved by choosing alternative sampling schedules. 4D ^{13}C NOESY sequences employ two HMQC/HSQC elements separated by a NOESY mixing period with either -^{13}C,^{13}C- or -^{13}C,^{15}N- variants.[71] The inclusion of a 2D heteronuclear correlation sequence before and after the NOE transfer significantly simplifies assignment as shown in Figure 7 where comparison with a 2D ^{13}C HMQC experiment allows easy assignment of the diagonal and cross-peaks, in contrast to the equivalent 3D H(C)CH or (H)CCH experiments. Dramatic improvements in resolution can be achieved by further increasing the evolution periods or by recording an RQD-NUS experiment. In the latter case, detection of only one quadrature component per complex point in the indirect dimensions allowed the resolution to be approximately doubled in each indirect dimension in the same experiment time, resulting in the observed higher resolution.[17] This could equivalently be achieved by sampling to higher resolution in the NUS experiment, using an alternative choice of sampling schedule, although it has been previously suggested that biasing the sampling schedule toward time- rather than quadrature components may have advantages for the reconstruction quality.[17] Therefore, RQD offers additional flexibility in defining a sampling schedule.

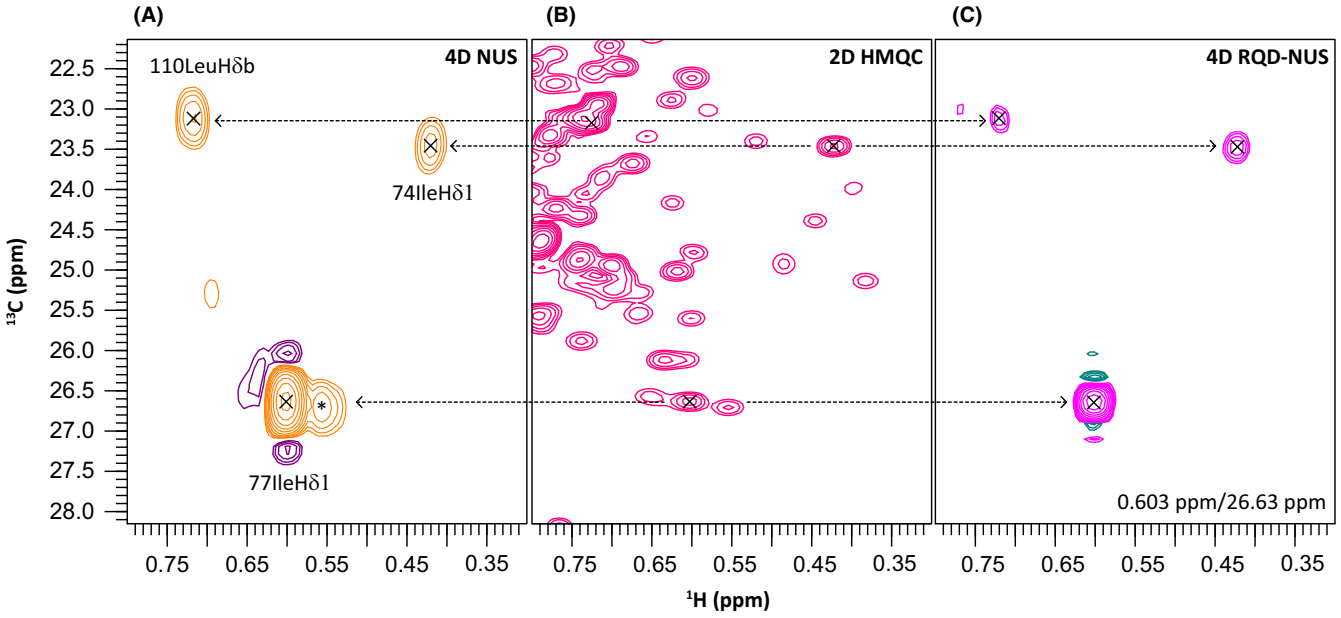

FIGURE 7 Reconstruction of a 4D HCCH-NOESY experiment recorded on a 0.3 mM U-[^{2}H,^{13}C,^{15}N] Ileδ1-[^{13}CH$_3$], Leu, Val-[^{13}CH$_3$, ^{12}CD$_3$], Ala-[^{13}CH$_3$] labelled sample of pSRII. CS-IHT reconstruction of an NUS spectrum recorded with 8% sampling and an equivalent t_{1max} of 15 ms (^{1}H), 10.5 ms (^{13}C) and 8.1 ms (^{13}C) (24* × 26* × 20* complex points with spectral widths of 1600 Hz, 2480 Hz and 2480 Hz in the indirect ^{1}H, ^{13}C and ^{13}C dimensions respectively) and ns = 40, giving an experiment time of ~4.5 days, is shown in A. The diagonal and cross peaks can be simply assigned by comparison with a 2D [^{1}H,^{13}C] HMQC experiment (B), acquired with 64* complex points in the ^{13}C dimension and ns = 8. C, shows a 4D RQD-NUS experiment (experiment time ~4.5 days) with CS$_{RQD}$ reconstruction, acquired with 1% overall sampling (8% NUS equivalent) and an equivalent t_{1max} of 28.8 ms (^{1}H), 21.0 ms (^{13}C) and 16.1 ms (^{13}C) (46* × 52* × 40* complex points with spectral widths of 1600 Hz, 2480 Hz and 2480 Hz in the indirect ^{1}H, ^{13}C and ^{13}C dimensions respectively) and ns = 40. * indicates breakthrough from another plane. Spectra were recorded at 298 K on a Bruker AV800 spectrometer equipped with a 5 mm TXI HCN/z cryoprobe.

10 | PRACTICAL TIPS

10.1 | Data acquisition

An essential component of acquiring undersampled NMR data is choosing an appropriate undersampling scheme. This requires careful selection of both the sampling fraction, which is related to the sparsity of the spectrum (ie, number of signals expected), as well as the distribution of points. Early work in the field proposed exponentially biased schemes allowing acquisition of more high SNR data points at early time points while maintaining some longer time points to provide sufficient resolution.[30] More recently, sine-weighted Poisson gap sampling (SPS) has been proposed, which maintains the biased selection of data points, but minimizes variability between different randomly generated sampling schedules.[31] Sampling using a Poisson-disk algorithm has also previously been proposed.[73] Using Poisson sampling is likely to minimize the chance of generating a "bad" schedule for a given set of input criteria. Poisson gap schedules can be generated using the hmsIST Schedule generator[74] (a version with more advanced options is available at http://gwagner.med.harvard.edu/intranet/hmsIST/gensched_old.html[13]) or using nussampler as part of the MDD software package.[75] Some guidelines have been suggested in the literature for appropriate sampling levels,[13,18] which may prove useful as a starting point. However, two important caveats must be considered. (a) As discussed earlier, Equation 15 shows that the sampling requirement is directly proportional to the sparsity, and proportional to log(N) where N is the number of points. Thus a particularly crowded spectrum will require more samples than a less crowded spectrum. (b) Percentage sampling factors can be misleading as they reflect the proportion of the total fully sampled grid which is selected; thus a very high-resolution spectrum could show a very low sampling percentage, but a lower resolution spectrum of the same protein would need a similar number of samples (based on Equation 15) giving a much higher percentage.

The best way to determine a suitable sampling level is to process a comparable fully sampled experiment with several different undersampling schemes with different fractional sampling levels, using the desired reconstruction method, and to assess the spectral quality against the fully sampled FT spectrum. This can be done using many of the available software packages.

When selecting a sampling schedule it is important to sample the first time point in all the indirect dimensions as this can help with phasing for the direct dimension, and allows the data collection to be checked as the first point should be equivalent to a fully sampled experiment. It is often useful to record a data point at the maximum increment in all indirect dimensions, as this allows easier identification of the maximum data size. As discussed earlier, randomization (ie, reducing regularity in the sampling schedule) typically reduces artifact levels[2] while clumps of data points, with large gaps elsewhere in the schedule should also be avoided, particularly if these occur at the beginning and end of the schedule (largely achieved by weighted Poisson sampling).[31] Exponential schedules can be generated using the NUS Schedule Tool, which provides a helpful GUI to visualize schedules, while the MDD-NMR nussampler provides options for Poisson sampling with matching to J-coupling or exponential decays.[75,76] Note that constant time dimensions do not need any decay and this option can be selected for appropriate dimensions in the various schedulers available (although the authors of SPS sampling still recommend a sinusoidal weight of 2).

10.2 | Data processing

A variety of software packages is available for CS reconstructions. These include:

10.2.1 | hmsIST

hmsIST comes from the Wagner lab[19] and is available on request. hmsIST functions as part of the NMRPipe workflow. A useful resource discussing NUS approaches, sampling schedules, pulse programmes, and a tutorial on data processing using nmrPipe and hmIST is available at http://gwagner.med.harvard.edu/intranet/hmsIST/

10.2.2 | NMRPipe

NMRPipe includes its own implementation of the IST algorithm similar to IST-D discussed above. More information is available at https://www.ibbr.umd.edu/nmrpipe/nus.html

10.2.3 | MddNMR

MddNMR is provided by the Swedish NMR Centre (Gothenburg)[16,77] and can be downloaded from the site http://mddnmr.spektrino.com/, where there is also an instruction manual, example data, and scripts. qMDD provides a graphical user interface to the MddNMR programme allowing easy editing of scripts. The package allows IST, IRLS, low-rank (for 2D spectra), and MDD (not covered in this review) reconstructions of NUS data and integrates with NMRPipe.

10.2.4 | NESTA-NMR

NESTA-NMR[52] implements the NESTA algorithm[78] allowing regularization using ℓ_1, reweighted ℓ_1 (IRL1), and

Gaussian smoothed ℓ_0 terms. It integrates with NMRPipe and can be accessed, along with documentation, at http://nestanmr.com/.

10.2.5 | Cambridge CS

Cambridge CS is provided by the authors and is available on request.[15,18] It implements a number of algorithms including ℓ_1-based methods (IHT and IST) as well as reweighted methods (IRL1). The programme uses a GUI to facilitate set-up of processing scripts. Full processing can be carried out in Cambridge CS but import from and export to the NMRPipe format is also possible.

10.2.6 | Bruker TopSpin

TopSpin implements versions of the IST and IRLS algorithms, along with MDD processing.

Many of the packages described above are available on NMRbox[79] enabling easy testing of the packages without the complexities of installing individual packages. In addition, many other packages are available for other NMR data processing methods which are not described in this review.

10.3 | Guidelines

While each processing package has its own particular requirements some general guidelines are presented here.

1. The general outline for NUS data processing is to process the data in the direct (acquisition dimension), which is fully sampled using the FFT. This is followed by reconstruction in the indirect dimension(s).
2. The direct dimension must be appropriately phased. This can be achieved by FFT in the direct dimension followed by viewing the data as a 2D cube and phasing the first row. However, most software allows full spectral processing using the FFT in all dimensions with zeros replacing the skipped points. This can simplify phase correction in the direct dimension and also allows the user to check that appropriate processing options have been applied in the indirect dimensions. For example, correct settings for frequency discrimination, phasing for any pre-calculated delays in the indirect dimensions and if necessary appropriate window functions, should be checked at this stage before starting CS reconstruction. We recommend this latter approach. The speed of the FFT, even for large datasets, means this is not a time-consuming approach.
3. Once correct settings have been identified for the indirect dimensions as described in 2., the processing method of choice can be applied. For 2D and 3D reconstructions, CS reconstruction times are on the order of seconds to minutes for a 2D and around 5-30 minutes for a 3D using standard computer hardware, with multithreading enabled, for example, Ref. 13. In all cases, reconstruction times can be shortened by limiting the maximum number of iterations. While this will be detrimental to the reconstruction quality, it can be used as a preliminary test to check that the reconstruction is proceeding correctly, before proceeding with full reconstruction. This may be particularly useful for 4D spectra where reconstruction times are on the order of hours, around 0.5-1 day for larger spectra.
4. Spectra can also be checked by processing during acquisition, although the quality of the spectral appearance will depend on the number of points acquired. Sampling lists can be produced in a randomized order: in this case, reconstruction before the experiment has completed provides a more realistic indication of the resolution, compared to an ordered list, since a mixture of longer and shorter time-points will have been acquired. In this case, it is also possible to stop acquisition earlier once the desired quality is achieved, although this requires an option in the processing software to ignore the unacquired data points during the reconstruction.

11 | CONCLUSION

Compressed sensing reconstruction techniques have become increasingly popular in NMR spectroscopy enabling spectroscopists to benefit from NUS sampling to carefully balance resolution, sensitivity and experiment time parameters. These approaches enable dramatic improvements in resolution compared to FT reconstruction, and allow researchers to access higher dimensional experiments, with the potential for new experiment types and increasingly rich data. Furthermore, due to the increased sampling requirements of high-field machines, these data processing techniques will enable the full benefits of such high-field spectrometers to be realized. A variety of different reconstruction algorithms can be used for CS reconstructions, which are implemented in a range of different readily available software packages. Many of these packages enable researchers to artificially generate an undersampled data set from a fully sampled one enabling testing of algorithms and sampling schedules before applying to "real" samples. CS-NUS reconstruction techniques are now in widespread use in NMR laboratories around the world and we anticipate many exciting developments in the years to come.

ACKNOWLEDGMENTS

The authors thank Robert Tovey and Dr. Bogdan Roman for useful discussions.

ORCID

Mark Bostock http://orcid.org/0000-0001-6717-5786
Daniel Nietlispach http://orcid.org/0000-0003-4364-9291

REFERENCES

1. Mobli M, Hoch JC. Nonuniform sampling and non-Fourier signal processing methods in multidimensional NMR. *Prog Nucl Magn Reson Spectrosc*. 2014;83:21-41.
2. Hoch JC, Maciejewski MW, Filipovic B. Randomization improves sparse sampling in multidimensional NMR. *J Magn Reson*. 2008;193:317-320.
3. Hiller S, Fiorito F, Wüthrich K, Wider G. Automated projection spectroscopy (APSY). *Proc Natl Acad Sci U S A*. 2005;102:10876-10881.
4. Kim S, Szyperski T. GFT NMR, a new approach to rapidly obtain precise high-dimensional NMR spectral information. *J Am Chem Soc*. 2003;125:1385-1393.
5. Malmodin D, Billeter M. Multiway decomposition of NMR spectra with coupled evolution periods. *J Am Chem Soc*. 2005;127:13486-13487.
6. Candès EJ, Romberg J, Tao T. Robust uncertainty principles: exact signal reconstruction from highly incomplete frequency information. *IEEE Trans Inf Theory*. 2006;52:489-509.
7. Donoho DL. Compressed sensing. *IEEE Trans Inf Theory*. 2006;52:1289-1306.
8. Logan BF. *Properties of High-Pass Signals*. New York, NY: Columbia University; 1965.
9. Lustig M, Donoho DL, Pauly JM. Sparse MRI: the application of compressed sensing for rapid MR imaging. *Magn Reson Med*. 2007;58:1182-1195.
10. Lustig M, Donoho DL, Santos JM, Pauly JM. Compressed sensing MRI. *IEEE Signal Process Mag*. 2008;25:72-82.
11. Wiaux Y, Jacques L, Puy G, Scaife AMM, Vandergheynst P. Compressed sensing imaging techniques for radio interferometry. *Mon Not R Astron Soc*. 2009;395:1733-1742.
12. Zhu L, Zhang W, Elnatan D, Huang B. Faster STORM using compressed sensing. *Nat Methods*. 2012;9:721-723.
13. Hyberts SG, Arthanari H, Robson SA, Wagner G. Perspectives in magnetic resonance: NMR in the post-FFT era. *J Magn Reson*. 2014;241:60-73.
14. Sanders JN, Saikin SK, Mostame S, Andrade X, Widom JR, Marcus AH, et al. Compressed sensing for multidimensional spectroscopy experiments. *J Phys Chem Lett*. 2012;3:2697-2702.
15. Holland DJ, Bostock MJ, Gladden LF, Nietlispach D. Fast multidimensional NMR spectroscopy using compressed sensing. *Angew Chem Int Ed Engl*. 2011;50:6548-6551.
16. Kazimierczuk K, Orekhov VY. Accelerated NMR spectroscopy by using compressed sensing. *Angew Chem Int Ed Engl*. 2011;50:5556-5559.
17. Bostock MJ, Holland DJ, Nietlispach D. Improving resolution in multidimensional NMR using random quadrature detection with compressed sensing reconstruction. *J Biomol NMR*. 2017;68:67-77.
18. Bostock MJ, Holland DJ, Nietlispach D. Compressed sensing reconstruction of undersampled 3D NOESY spectra: application to large membrane proteins. *J Biomol NMR*. 2012;54:15-32.
19. Hyberts SG, Milbradt AG, Wagner AB, Arthanari H, Wagner G. Application of iterative soft thresholding for fast reconstruction of NMR data non-uniformly sampled with multidimensional Poisson Gap scheduling. *J Biomol NMR*. 2012;52:315-327.
20. Kazimierczuk K, Orekhov VY. A comparison of convex and non-convex compressed sensing applied to multidimensional NMR. *J Magn Reson*. 2012;223:1-10.
21. Lin EC, Opella SJ. Sampling scheme and compressed sensing applied to solid-state NMR spectroscopy. *J Magn Reson*. 2013;237:40-48.
22. Mayzel M, Kazimierczuk K, Orekhov VY. The causality principle in the reconstruction of sparse NMR spectra. *Chem Commun (Camb)*. 2014;50:8947-8950.
23. Shchukina A, Kasprzak P, Dass R, Nowakowski M, Kazimierczuk K. Pitfalls in compressed sensing reconstruction and how to avoid them. *J Biomol NMR*. 2017;68:79-98.
24. Thiele CM, Bermel W. Speeding up the measurement of one-bond scalar (^1J) and residual dipolar couplings (^1D) by using non-uniform sampling (NUS). *J Magn Reson*. 2012;216:134-143.
25. Urbańczyk M, Nowakowski M, Koźmiński W, Kazimierczuk K. Joint non-uniform sampling of all incremented time delays for quicker acquisition in protein relaxation studies. *J Biomol NMR*. 2017;68:155-161.
26. Urbańczyk M, Bernin D, Koźmiński W, Kazimierczuk K. Iterative thresholding algorithm for multiexponential decay applied to PGSE NMR data. *Anal Chem*. 2013;85:1828-1833.
27. Hoch JC, Stern AS. *NMR Data Processing*. New York, NY: Wiley-Liss; 1996.
28. Rovnyak D, Hoch JC, Stern AS, Wagner G. Resolution and sensitivity of high field nuclear magnetic resonance spectroscopy. *J Biomol NMR*. 2004;30:1-10.
29. Szyperski T, Yeh DC, Sukumaran DK, Moseley HNB, Montelione GT. Reduced-dimensionality NMR spectroscopy for high-throughput protein resonance assignment. *Proc Natl Acad Sci U S A*. 2002;99:8009-8014.
30. Barna JCJ, Laue ED, Mayger MR, Skilling J, Worrall SJP. Exponential sampling, an alternative method for sampling in two-dimensional NMR experiments. *J Magn Reson*. 1987;73:69-77.
31. Hyberts SG, Takeuchi K, Wagner G. Poisson-gap sampling and forward maximum entropy reconstruction for enhancing the resolution and sensitivity of protein NMR data. *J Am Chem Soc*. 2010;132:2145-2147.
32. Kazimierczuk K, Zawadzka A, Koźmiński W, Zhukov I. Lineshapes and artifacts in Multidimensional Fourier Transform of arbitrary sampled NMR data sets. *J Magn Reson*. 2007;188:344-356.
33. Högbom JA. Aperture synthesis with a non-regular distribution of interferometer baselines. *Astron Astrophys Suppl*. 1974;15:417-426.
34. Coggins BE, Zhou P. High resolution 4-D spectroscopy with sparse concentric shell sampling and FFT-CLEAN. *J Biomol NMR*. 2008;42:225-239.
35. Coggins BE, Werner-Allen JW, Yan AK, Zhou P. Rapid protein global fold determination using ultrasparse sampling, high-

dynamic range artifact suppression, and time-shared NOESY. *J Am Chem Soc*. 2012;134:18619-18630.
36. Stanek J, Koźmiński W. Iterative algorithm of discrete Fourier transform for processing randomly sampled NMR data sets. *J Biomol NMR*. 2010;47:65-77.
37. Sibisi S, Skilling J, Brereton RG, Laue ED, Staunton J. Maximum entropy signal processing in practical NMR spectroscopy. *Nature*. 1984;311:446-447.
38. Barna JCJ, Laue ED. Conventional and exponential sampling for 2D NMR experiments with application to a 2D NMR spectrum of a protein. *J Magn Reson*. 1987;75:384-389.
39. Rovnyak D, Frueh DP, Sastry M, Sun Z-YJ, Stern AS, Hoch JC, et al. Accelerated acquisition of high resolution triple-resonance spectra using non-uniform sampling and maximum entropy reconstruction. *J Magn Reson*. 2004;170:15-21.
40. Hoch JC, Stern AS. Maximum Entropy Reconstruction, Spectrum Analysis and Deconvolution in Multidimensional Nuclear Magnetic Resonance. *Methods in Enzymology*. 2002;338:159-178.
41. Mobli M, Hoch JC. Maximum entropy spectral reconstruction of nonuniformly sampled data. *Concepts Magn Reson Part A*. 2008;32A:436-448.
42. Orekhov VY, Ibraghimov IV, Billeter M. MUNIN: a new approach to multi-dimensional NMR spectra interpretation. *J Biomol NMR*. 2001;20:49-60.
43. Tugarinov V, Kay LE, Ibraghimov I, Orekhov VY. High-resolution four-dimensional ^{1}H-^{13}C NOE spectroscopy using methyl-TROSY, sparse data acquisition, and multidimensional decomposition. *J Am Chem Soc*. 2005;127:2767-2775.
44. Orekhov VY, Ibraghimov I, Billeter M. Optimizing resolution in multidimensional NMR by three-way decomposition. *J Biomol NMR*. 2003;27:165-173.
45. Jaravine V, Ibraghimov I, Yu OV. Removal of a time barrier for high-resolution multidimensional NMR spectroscopy. *Nat Methods*. 2006;3:605-607.
46. Hiller S, Ibraghimov I, Wagner G, Orekhov VY. Coupled decomposition of four-dimensional NOESY spectra. *J Am Chem Soc*. 2009;131:12970-12978.
47. Szyperski T, Wider G, Bushweller J, Wüthrich K. 3D ^{13}C-^{15}N-heteronuclear two-spin coherence spectroscopy for polypeptide backbone assignments in ^{13}C-^{15}N-double-labeled proteins. *J Biomol NMR*. 1993;3:127-132.
48. Kupče Ē, Freeman R. Projection-reconstruction of three-dimensional NMR spectra. *J Am Chem Soc*. 2003;125:13958-13959.
49. Atreya HS, Szyperski T. G-matrix Fourier transform NMR spectroscopy for complete protein resonance assignment. *Proc Natl Acad Sci U S A*. 2004;101:9642-9647.
50. Kazimierczuk K, Stanek J, Zawadzka-Kazimierczuk A, Koźmiński W. Random sampling in multidimensional NMR spectroscopy. *Prog Nucl Magn Reson Spectrosc*. 2010;57:420-434.
51. Natarajan BK. Sparse approximate solutions to linear systems. *SIAM J Comput*. 1995;24:227-234.
52. Sun S, Gill M, Li Y, Huang M, Byrd RA. Efficient and generalized processing of multidimensional NUS NMR data: the NESTA algorithm and comparison of regularization terms. *J Biomol NMR*. 2015;62:105-117.
53. Stern AS, Donoho DL, Hoch JC. NMR data processing using iterative thresholding and minimum l_1-norm reconstruction. *J Magn Reson*. 2007;188:295-300.
54. Drori I. Fast l_1 minimization by iterative thresholding for multidimensional NMR spectroscopy. *EURASIP J Adv Signal Process*. 2007;2007:20248.
55. Candès EJ, Wakin MB, Boyd SP. Enhancing sparsity by reweighted ℓ_1 minimization. *J Fourier Anal Appl*. 2008;14:877-905.
56. Chartrand R, Wotao Y. Iteratively reweighted algorithms for compressive sensing. *Proc IEEE Int Conf Acoust Speech Signal Process*. 2008;2008:3869-3872.
57. Yagle AE. Non-iterative reweighted-norm least-squares local l_0 Minimization for sparse solutions to underdetermined linear systems of equations. [Internet]. 2009 [cited 2017 Nov 27]. http://web.eecs.umich.edu/~aey/sparse/sparse11.pdf. Accessed June 13, 2018.
58. Chartrand R. Exact reconstruction of sparse signals via nonconvex minimization. *IEEE Signal Process Lett*. 2007;14:707-710.
59. Qu X, Guo D, Cao X, Cai S, Chen Z. Reconstruction of self-sparse 2D NMR spectra from undersampled data in the indirect dimension. *Sensors*. 2011;11:8888-8909.
60. Qu X, Mayzel M, Cai J-F, Chen Z, Orekhov V. Accelerated NMR spectroscopy with low-rank reconstruction. *Angew Chem Int Ed Engl*. 2015;54:852-854.
61. Ying J, Lu H, Wei Q, Cai J-F, Guo D, Wu J, et al. Hankel matrix nuclear norm regularized tensor completion for *N*-dimensional exponential signals. *IEEE Trans Signal Process*. 2017;65:3702-3717.
62. Cai J-F, Candès EJ, Shen Z. A singular value thresholding algorithm for matrix completion. *SIAM J Optim*. 2010;20:1956-1982.
63. Hyberts SG, Robson SA, Wagner G. Interpolating and extrapolating with hmsIST: seeking a t_{max} for optimal sensitivity, resolution and frequency accuracy. *J Biomol NMR*. 2017;68:139-154.
64. Salzmann M, Pervushin K, Wider G, Senn H, Wüthrich K. TROSY in triple-resonance experiments: new perspectives for sequential NMR assignment of large proteins. *Proc Natl Acad Sci U S A*. 1998;95:13585-13590.
65. Misiak M, Koźmiński W, Chmurski K, Kazimierczuk K. Study of near-symmetric cyclodextrins by compressed sensing 2D NMR. *Magn Reson Chem*. 2013;51:110-115.
66. Maciejewski MW, Fenwick M, Schuyler AD, Stern AS, Gorbatyuk V, Hoch JC. Random phase detection in multidimensional NMR. *Proc Natl Acad Sci U S A*. 2011;108:16640-16644.
67. Schuyler AD, Maciejewski MW, Stern AS, Hoch JC. Nonuniform sampling of hypercomplex multidimensional NMR experiments: dimensionality, quadrature phase and randomization. *J Magn Reson*. 2015;254:121-130.
68. Zawadzka-Kazimierczuk A, Kazimierczuk K, Koźmiński W. A set of 4D NMR experiments of enhanced resolution for easy resonance assignment in proteins. *J Magn Reson*. 2010;202:109-116.
69. Mobli M, Stern AS, Bermel W, King GF, Hoch JC. A non-uniformly sampled 4D HCC(CO)NH-TOCSY experiment processed using maximum entropy for rapid protein sidechain assignment. *J Magn Reson*. 2010;204:160-164.
70. Stanek J, Augustyniak R, Koźmiński W. Suppression of sampling artefacts in high-resolution four-dimensional NMR spectra using signal separation algorithm. *J Magn Reson*. 2012;214:91-102.

71. Kazimierczuk K, Stanek J, Zawadzka-Kazimierczuk A, Koźmiński W. High-dimensional NMR spectra for structural studies of biomolecules. *ChemPhysChem*. 2013;14:3015-3025.
72. Kosiński K, Stanek J, Górka MJ, Żerko S, Koźmiński W. Reconstruction of non-uniformly sampled five-dimensional NMR spectra by signal separation algorithm. *J Biomol NMR*. 2017;68:129-138.
73. Kazimierczuk K, Zawadzka A, Koźmiński W. Optimization of random time domain sampling in multidimensional NMR. *J Magn Reson*. 2008;192:123-130.
74. hmsIST schedule generator. [Internet]. [cited 2017 Oct 16]. http://gwagner.med.harvard.edu/intranet/hmsIST/gensched_new.html. Accessed June 13, 2018.
75. MddNMR-home. [Internet]. [cited 2017 Oct 16]. http://mddnmr.spektrino.com/. Accessed June 13, 2018.
76. Sample scheduler for non-uniform data sets. [Internet]. [cited 2017 Oct 16]. http://sbtools.uchc.edu/nmr/sample_scheduler/. Accessed June 13, 2018.
77. Orekhov VY, Jaravine VA. Analysis of non-uniformly sampled spectra with multi-dimensional decomposition. *Prog Nucl Magn Reson Spectrosc*. 2011;59:271-292.
78. Becker S, Bobin J, Candès E. NESTA: a fast and accurate first-order method for sparse recovery. *SIAM J Imaging Sci*. 2009;4:1-39.
79. Maciejewski MW, Schuyler AD, Gryk MR, Moraru II, Romero PR, Ulrich EL, et al. NMRbox: a resource for biomolecular NMR computation. *Biophys J* . 2017;112:1529-1534.

How to cite this article: Bostock M, Nietlispach D. Compressed sensing: Reconstruction of non-uniformly sampled multidimensional NMR data. *Concepts Magn Reson Part A*. 2018;46A:e21438. https://doi.org/10.1002/cmr.a.21438